scientific reports

OPEN

SMC translocation is unaffected by an excess of nucleoid associated proteins in vivo

Zhongqing Ren[1,2,3], Lindsey E. Way[1,3] & Xindan Wang[1✉]

Genome organization is important for DNA replication, gene expression, and chromosome segregation. In bacteria, two large families of proteins, nucleoid-associated proteins (NAPs) and SMC complexes, play important roles in organizing the genome. NAPs are highly abundant DNA-binding proteins that can bend, wrap, bridge, and compact DNA, while SMC complexes load onto the chromosome, translocate on the DNA, and extrude DNA loops. Although SMC complexes are capable of traversing the entire chromosome bound by various NAPs in vivo, it is unclear whether SMC translocation is influenced by NAPs. In this study, using *Bacillus subtilis* as a model system, we expressed a collection of representative bacterial and archaeal DNA-binding proteins that introduce distinct DNA structures and potentially pose different challenges for SMC movement. By fluorescence microscopy and chromatin immunoprecipitation, we observed that these proteins bound to the genome in characteristic manners. Using genome-wide chromosome conformation capture (Hi-C) assays, we found that the SMC complex traversed these DNA-binding proteins without slowing down. Our findings revealed that the DNA-loop-extruding activity of the SMC complex is unaffected by exogenously expressed DNA-binding proteins, which highlights the robustness of SMC motors on the busy chromatin.

Keywords SMC, NAP, Nucleoid-associated proteins, HU, HBsu, H-NS, HMfA, HMfB, Loop extrusion, *Bacillus subtilis*

Chromosomes are highly organized to allow biological processes and enable faithful DNA segregation. The Structural Maintenance of Chromosomes (SMC) complex is a major chromosome organizer in all three domains of life[1,2]. For example, eukaryotic SMC cohesins mediate self-associated domains during interphase and sister chromatid cohesion before chromosome segregation[3,4]; eukaryotic SMC condensins compact the DNA and facilitate proper chromosome segregation during mitosis[5,6]; bacterial SMC complexes are critical for the resolution of two newly replicated sister chromosomes[7–11]; the archaeal SMC analog, coalescin, mediates chromosome compartmentalization and regulates gene expression[12]. Despite performing different functions, SMC complexes have highly conserved structure, indicating a conserved molecular mechanism for action.

In recent years, in vivo studies in eukaryotes and bacteria have provided evidence that SMC complexes extrude DNA loops[8,10,13–15]. In the case of *Bacillus subtilis*, SMC complexes are loaded at centromeric *parS* sites near the replication origin by the partitioning protein ParB[16–18]. Once loaded, SMC complexes translocate away from the loading site while tethering the two arms together, generating inter-chromosome arm (inter-arm) interactions[8,10,19,20]. Although the *B. subtilis* SMC complex has not been shown to extrude DNA loops in vitro, single-molecule experiments have shown that purified eukaryotic SMC complexes and bacterial SMC Wadjet complexes load onto the chromosome and generate a small DNA loop, then translocate away from the loading site in an ATP hydrolysis–dependent manner, processively enlarging the loop[21–26].

The loop-extrusion model presents an elegantly simple mechanism for SMC-mediated chromosome resolution. However, it also raises a number of important questions regarding the proteins on the chromosome and the DNA transactions that occur in vivo. The chromosome is a very busy molecule full of possible roadblocks for SMC to encounter. Such roadblocks include DNA-binding proteins, replisomes, RNA polymerases, complex DNA structures, and more. A previous study has shown that in *B. subtilis*, RNA polymerases act as moving barriers against SMC translocation, and the effect is correlated with the direction and level of transcription[27]. Similarly, in budding yeast, DNA arrays bound by the telomeric protein, Rap1, strongly affect SMC loop

[1]Department of Biology, Indiana University, 1001 E 3rd Street, Bloomington IN 47405, USA. [2]Molecular Biology Program, Memorial Sloan Kettering Cancer Center, New York NY 10065, USA. [3]Zhongqing Ren, Lindsey E. Way These authors contributed equally. ✉email: xindan@iu.edu

1

extrusion in vitro and in vivo[28]. It is unclear whether other protein machineries on the chromatin hinder SMC translocation.

The most abundant proteins on the bacterial chromosome are nucleoid-associated proteins (NAPs). HU protein is a well-conserved NAP among bacterial species[29]. In *E. coli*, the two HU proteins, HupA and HupB, primarily form heterodimers and bind to DNA non-specifically[30,31]. HU has been shown to induce flexible bends in DNA over a range of angles[32,33] (Fig. 1a). In vitro, high concentrations of HU lead to cooperative binding and formation of rigid nucleoprotein filaments[32,34,35]. H-NS is another well-characterized NAP. H-NS preferentially binds to AT-rich, kinked, and xenogeneic DNA[36]. It forms homodimers that can engage in further dimer-dimer interactions, allowing this protein to form nucleoprotein filaments[37,38]. Moreover, H-NS molecules binding at distant loci interact to form DNA bridges[38–40] (Fig. 1a). These actions of H-NS seclude AT-rich portions of the genome from RNA polymerase or transcriptional activators, thereby repressing transcription[38,40,41].
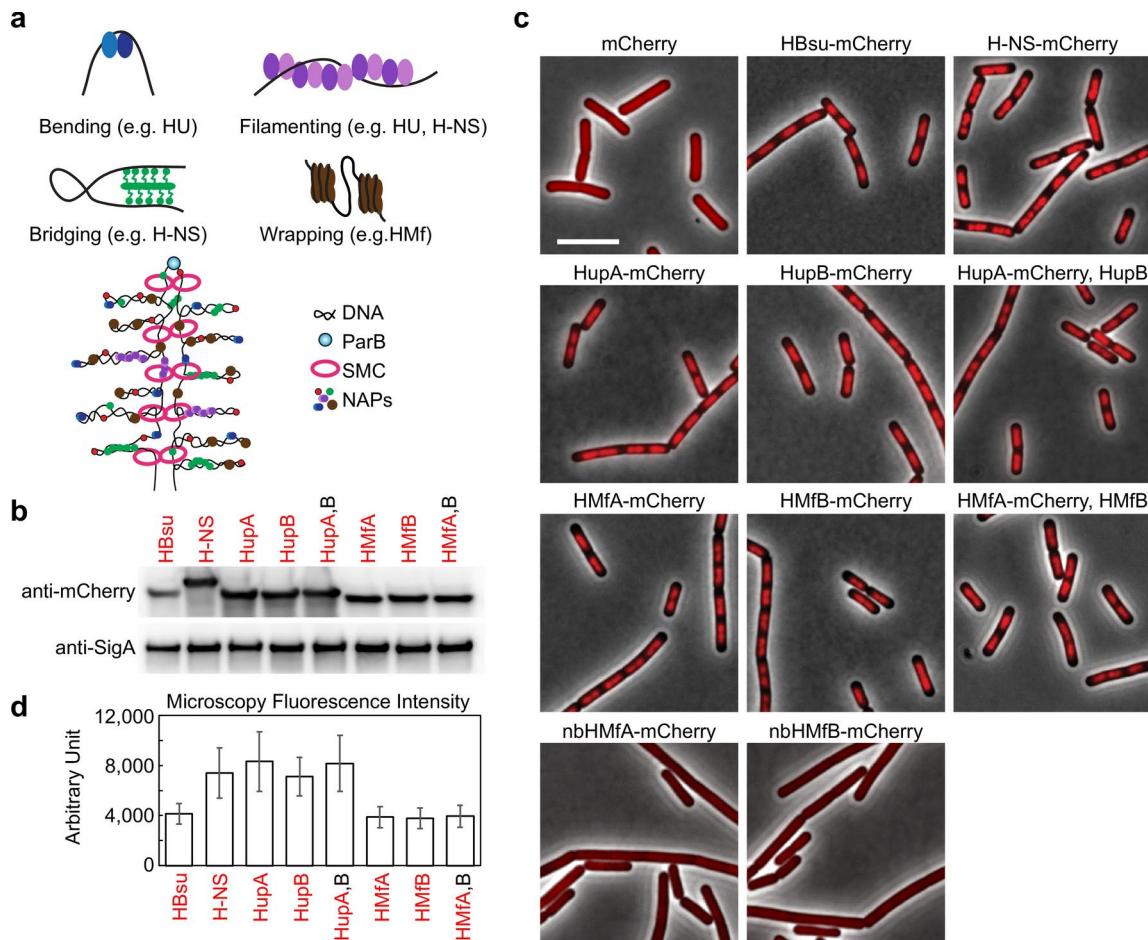

Fig. 1. Exogenous DNA-binding proteins are expressed and localized to the nucleoid. (**a**) The experimental setup of this study. Schematic representation of DNA-binding proteins bending DNA, forming filaments on DNA, bridging distal DNA segments, or wrapping the DNA and introducing nucleosome-like structures. In this study, we express prokaryotic DNA-binding proteins in *B. subtilis* and test their effect on SMC translocation. (**b**) Immunoblot analysis of protein expression. HBsu-mCherry (BWX523) was expressed from *hbs*' native promoter as a merodiploid at an ectopic locus. H-NS-mCherry (BWX5256), HupA-mCherry (BWX5269), HupB-mCherry (BWX5271), HupA-mCherry/HupB dimer (BWX5598), HMfA-mCherry (BWX5427), HMfB-mCherry (BWX5429), HMfA-mCherry/HMfB dimer (BWX5600) were induced by 0.5% xylose for 90 min. Red writing indicates the proteins that are tagged with mCherry. The samples were probed with mCherry polyclonal antibodies. SigA was used as a loading control. Uncropped gels can be found in Supplementary Information. (**c**) Exogenous DNA-binding proteins localize to the nucleoid. Fluorescence microscopy of *B. subtilis* expressing the indicated proteins. HBsu-mCherry (BWX523) was expressed from *hbs*' native promoter as a merodiploid at an ectopic locus. Untagged mCherry (BWX5560), H-NS-mCherry (BWX5256), HupA-mCherry (BWX5269), HupB-mCherry (BWX5271), HupA-mCherry/HupB dimer (BWX5598), HMfA-mCherry (BWX5427), HMfB-mCherry (BWX5429), HMfA-mCherry/HMfB dimer (BWX5600), nbHMfA-mCherry (BWX5947), or nbHMfB-mCherry (BWX5949) was induced with 0.5% xylose for 90 min. Scale bar represents 4 μm. (**d**) Quantification of fluorescence intensity in (**c**). The mean pixel intensities were plotted as histograms. Error bars indicate the standard deviation of pixel intensity. Red writing indicates the proteins that are tagged with mCherry.

Archaeal species also have abundant DNA-binding proteins that organize the chromosome. For example, the HMf proteins (HMfA and HMfB) of *Methanothermus fervidus* oligomerize into tetrameric histone-like structures that wrap 60 bp of DNA[42,43] (Fig. 1a). Cooperative binding of additional HMf subunits to the tetrameric structure results in extended hypernucleosomes that wrap longer segments of DNA[43,44]. HMfs preferentially bind to DNA regions with a high G-C content and wrap the DNA helix[42,45]. HMfs have a high occupancy not only on the *M. fervidus* chromosome[46], but also when heterologously expressed in *E. coli*[47]. The large HMf-DNA nucleoprotein complex and the DNA architecture it creates may present challenges for motor proteins that act on DNA, such as SMC complexes.

In this study, we aim to investigate the effect of DNA-binding proteins on SMC translocation in *B. subtilis* in vivo (Fig. 1a). We expressed a representative sample of prokaryotic DNA-binding proteins that vary in sequence specificity, oligomerization state, and nucleoprotein complex structure, thus presenting varying challenges to the SMC complex during loop extrusion. Combining fluorescence microscopy, chromosome immunoprecipitation (ChIP-seq) and chromosome conformation assays (Hi-C), we investigated the cellular localizations and genome-wide binding profiles of these DNA-binding proteins and test how they affect the loop-extrusion activity of the SMC complex.

Results

Choosing a collection of DNA-binding proteins to express in *Bacillus subtilis*

To detect the impact of chromosome-binding proteins on translocation of the SMC complex on the chromosome, we expressed a collection of bacterial and archaeal DNA-binding proteins in *B. subtilis* and tracked SMC movement. We chose HU and H-NS from *E. coli* and HMf from *M. fervidus* (Fig. 1a) because of their DNA-sequence preferences, actions on DNA, and the chromosome architectures they create: HU binds the DNA non-specifically and bends the DNA[30–33]; H-NS binds AT-rich sequences, oligomerizes on DNA, and bridges distant DNA segments[36–39]; HMf preferentially binds GC-rich sequences and wraps DNA[47–49] (Fig. 1a). Since HU proteins have two subunits, HupA and HupB, which are capable of forming homodimers or heterodimers, we constructed three different strains to express HupA or HupB alone, or HupA and HupB as a heterodimer. Similarly, for HMf, we constructed three different strains to express HMfA or HMfB alone, or co-express HMfA and HMfB.

These proteins were fused to mCherry and expressed as a single copy from the *B. subtilis* chromosome under a xylose-inducible promoter (Pxyl). We used the mCherry fusions because they allowed for visualization of protein localization in living cells. More importantly, since NAPs are conserved proteins, the antibodies raised against *E. coli* NAPs might cross react with homologous proteins in *B. subtilis*. However, antibodies against mCherry enabled specific detection of the tagged proteins for Western Blotting and ChIP-seq. Using the same tag for different proteins also allowed us to quantify their expression levels and compare their genome-wide binding profiles. Finally, Pxyl allowed us to tune expression to the desired levels.

Exogenous DNA-binding proteins are expressed and localized to the nucleoid

To express the DNA-binding proteins at a sufficient but still physiologically relevant level, we used the expression level of a native *B. subtilis* NAP, the HU homolog HBsu[50], as a guide. HBsu is one of the most abundant proteins in *B. subtilis*[51,52], having ~ 20,000 monomers per cell[53]. For direct comparison, we fused HBsu to mCherry and expressed it under the native *hbs* promoter at an ectopic location. Immunoblot analysis using mCherry antibodies showed that after 90 min induction with 0.5% xylose, the exogenous DNA-binding proteins were expressed at levels higher than or similar to that of HBsu-mCherry (Fig. 1b). We used this induction condition for all of our experiments.

To examine the cellular localization of the exogenous DNA-binding proteins, we performed fluorescence microscopy. As controls, untagged mCherry localized throughout the volume of the cell, and *B. subtilis*' native NAP HBsu, when tagged with mCherry, localized to the nucleoid (Fig. 1c). When expressed in *B. subtilis*, mCherry-tagged H-NS, HupA, HupB, HMfA, HMfB, HupA-HupB heterodimer, and HMfA-HMfB heterodimer all localized to the nucleoid (Fig. 1c). When quantified, the intensity of the fluorescence signal of these exogenous proteins was higher than or similar to that of HBsu-mCherry (Fig. 1d), consistent with immunoblot analysis (Fig. 1b). Importantly, mCherry fusions to the mutants that were defective in DNA binding, nbHMfA and nbHMfB, both of which had three amino acid substitutions (K13T, R19S, T54K)[47,54], did not show nucleoid localization (Fig. 1c). Thus, nucleoid localization was a good indicator of DNA binding. These results show that all tagged proteins were expressed to appropriate levels and bound to the *B. subtilis* nucleoid.

Genome-wide binding profiles of the exogenous DNA-binding proteins

To investigate the binding profiles of the proteins of interest on the *B. subtilis* genome, we performed Chromatin Immunoprecipitation (ChIP-seq) assays (Fig. 2). For comparison, we did ChIP-seq on WT *B. subtilis* using anti-HBsu antibodies (Fig. 2a), and on the HBsu-mCherry-expressing strain using anti-mCherry antibodies (Fig. 2b). Except for sharp peaks at ribosomal RNA operons and other highly transcribed genes, which were likely caused by technical bias of ChIP-seq[10,55] (Fig. 2b), untagged HBsu and HBsu-mCherry showed a uniform binding profile along the genome, which was also evident when zoomed in to 100-kb or 10-kb regions. These results are consistent with the idea that HBsu binds to the genome in a non-specific manner. It further shows that the mCherry tag does not change the pattern of enrichment of HBsu on the genome. *E. coli* HupA-mCherry, HupB-mCherry, and the HupA-mCherry/HupB heterodimer showed the same non-specific binding profile as HBsu-mCherry (Figs. 2c, 2d and 2e).

In contrast, H-NS-mCherry had 678 enrichment peaks along the genome (Fig. 2f). The average GC content of the highest 100 peaks was 28.9%, much lower than the *B. subtilis* genome GC content (43.5%). These results are consistent with H-NS preferring AT-rich regions. Since *B. subtilis* has an H-NS-like protein, Rok, we performed
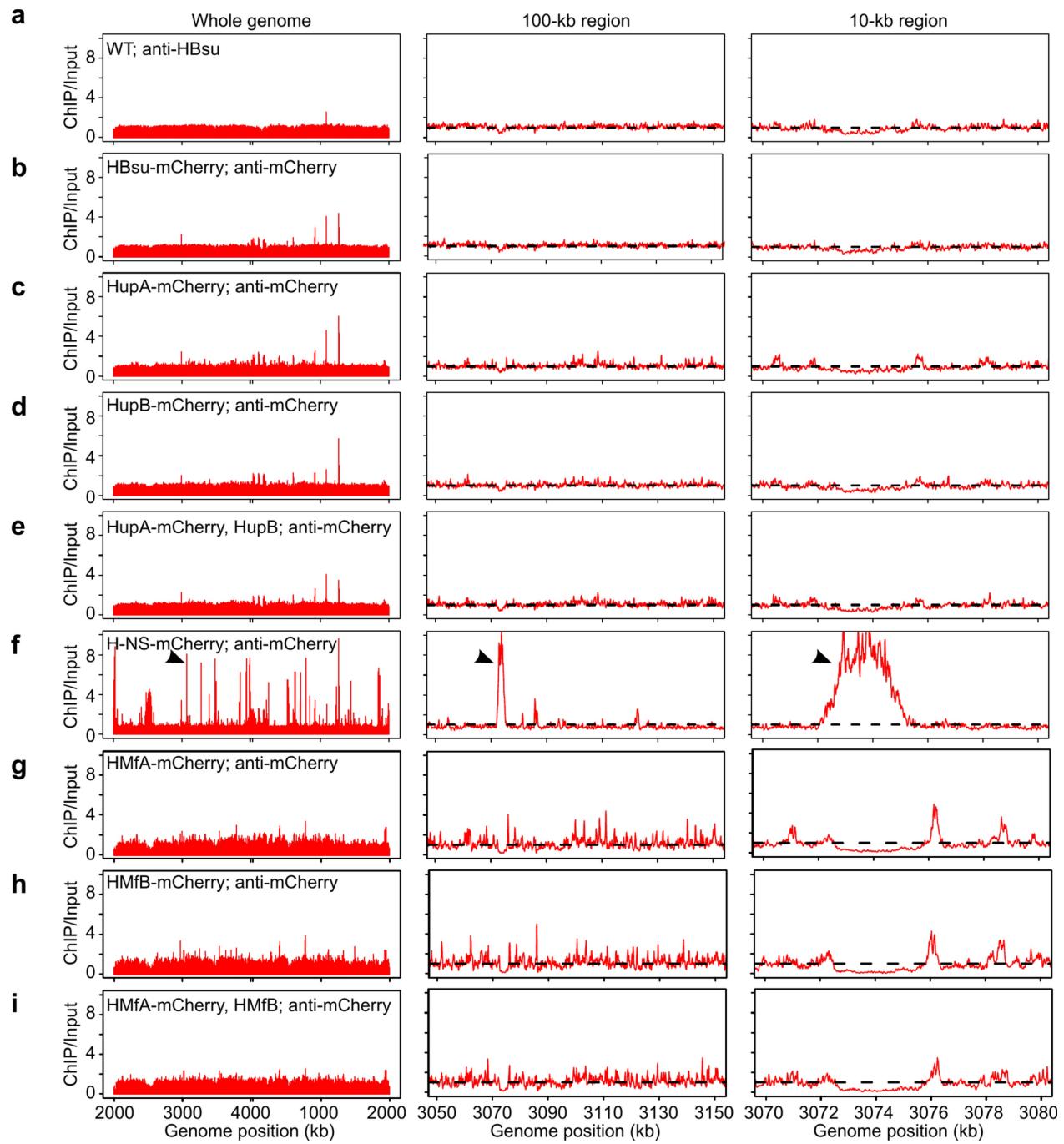
Fig. 2. Genome-wide DNA-binding profiles of indicated proteins by ChIP-seq. For each sample, the sequencing reads at each base pair position were normalized to the total number of reads before plotting. ChIP enrichment (ChIP over Input) was shown. The left panel was the profile of the whole genome binned at 1-kb resolution. The middle and right panels showed a 100-kb region (3050–3150 kb) and a 10-kb region (3070–3080 kb), both of which were binned at 100-bp resolution. The horizontal black dotted lines in 100-kb and 10-kb plots represented a ChIP/input enrichment value of 1. (**a**) Anti-HBsu ChIP-seq on WT *B. subtilis* (PY79). (**b**) Anti-mCherry ChIP-seq on HBsu-mCherry (BWX523) expressed from native *hbs* promoter at an ectopic location. (**c-i**) Anti-mCherry ChIP-seq on HupA-mCherry (BWX5269), HupB-mCherry (BWX5271), HupA-mCherry/HupB dimer (BWX5598), H-NS-mCherry (BWX5256), HMfA-mCherry (BWX5427), HMfB-mCherry (BWX5429), HMfA-mCherry/HMfB dimer (BWX5600). Expression of these proteins was induced with 0.5% xylose for 90 min. Black carets in (**f**) indicated the same peak on different plots.

anti-Rok ChIP-seq in WT *B. subtilis* for comparison[56]. Strikingly, H-NS-mCherry and Rok displayed virtually the same binding profile (**Figs. S1a and S1b**). These results indicate that H-NS family proteins have conserved DNA-binding specificity, and mCherry does not affect H-NS binding to the *B. subtilis* genome.

Finally, HMfA, HMfB, and the HMfA/B heterodimer displayed very similar binding profiles, with small enrichment peaks every 1–2 kilobasepairs, frequently at intergenic regions (Figs. 2g, 2h, and 2i). The average GC content of the highest 100 peaks was 52.3%, much higher than the *B. subtilis* genome GC content (43.5%). These results are consistent with the preference of HMfA and HMfB for GC-rich regions.

Overall, these ChIP-seq experiments showed that our chosen DNA-binding proteins, HupA, HupB, H-NS, HMfA, and HMfB, have expected characteristic binding specificities throughout the genome.

Effects of exogenous DNA-binding proteins on genome structure

To examine the effects of these proteins on *B. subtilis* chromosome organization, we performed chromosome conformation capture (Hi-C) assays on the strains expressing HupA-mCherry, HupB-mCherry, the HupA-mCherry/HupB heterodimer, HNS-mCherry, HMfA-mCherry, HMfB-mCherry, or the HMfA-mCherry/HMfB heterodimer, as well as a control strain not expressing these proteins (Fig. 3). All of these strains contained a single *parS* site at the origin. For the Hi-C procedure, we used a four-base cutter, DpnII, and achieved 1-kb resolution for DNA contacts.

Hi-C contact maps of these strains showed no observable difference (Fig. 3a). To quantify the interaction frequencies, we plotted the contact probability decay curve, Pc(s), which showed the average contact frequency
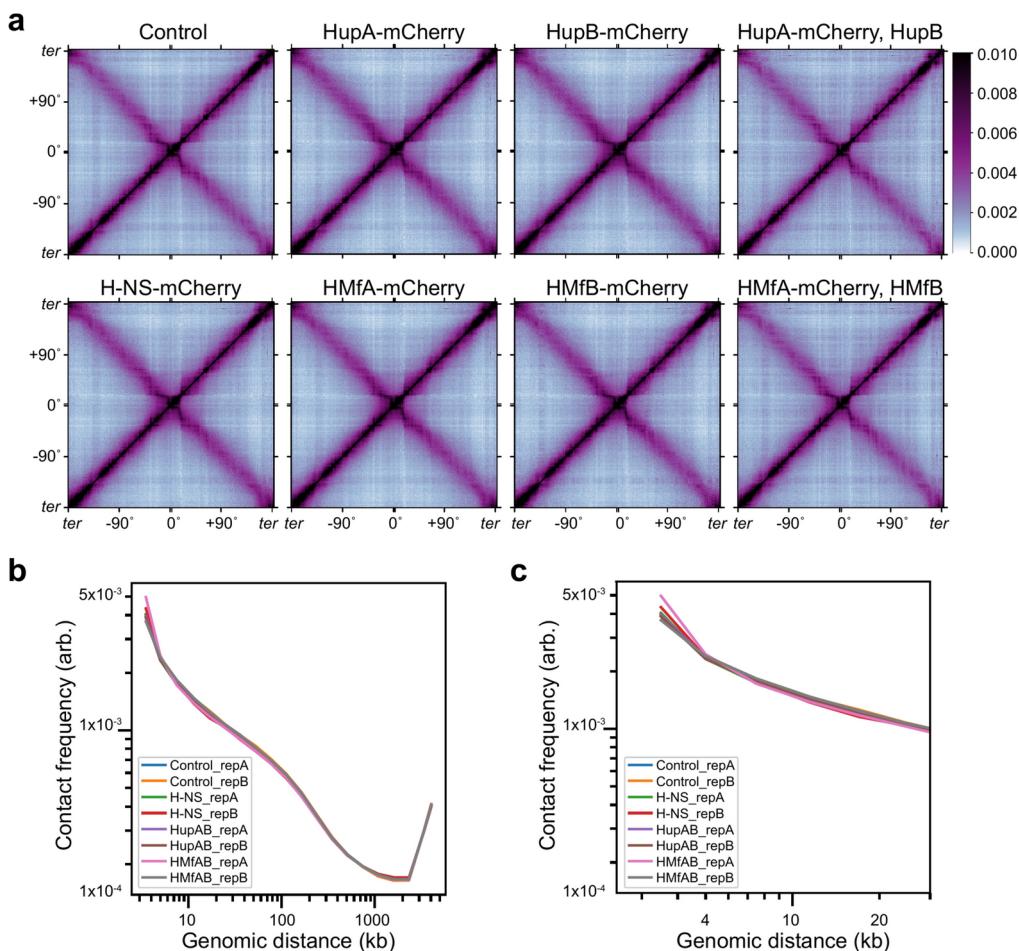

Fig. 3. Effects of exogenous DNA-binding proteins on genome folding. (**a**) Normalized Hi-C contact maps of the control strain (BWX3370) and strains expressing indicated proteins: HupA-mCherry (BWX5492), HupB-mCherry (BWX5494), the HupA-mCherry/HupB heterodimer (BWX5556), H-NS-mCherry (BWX5490), HMfA-mCherry (BWX5496), HMfB-mCherry (BWX5498), and the HMfA-mCherry/HMfB heterodimer (BWX5558). The contact maps were centered at the replication origin (0°). The fluorescence proteins were induced with 0.5% xylose for 90 min. The color scale bar on the right depicted Hi-C interaction scores for all contact maps shown in this study. (**b**) Contact probability Pc(s) curves showing the average contact frequency between all pairs of loci on the chromosome separated by a set distance (s). The x-axis indicated the genomic distance of separation in kb. The y-axis represented the averaged contact frequency. The curves were computed for interactions binned at 1 kb. Two biological replicates of each strain were shown. (**c**) High-resolution plots of Pc(s) curves showing interaction ranges from 2–30 kb.

between all pairs of loci on the chromosome separated by a set distance (s) (Fig. 3b). Two biological replicates of four strains (control, H-NS-mCherry, HupA-mCherry/HupB dimer, and the HMfA-mCherry/HMfB heterodimer) were analyzed. For loci separated by less than 4 kb, although the contact probabilities seemed variable between the strains, the differences were not reproducible in biological replicates of the same strains (Figs. 3b and 3c). For loci separated by 4 kb or more, the contact probabilities in different strains showed reproducible overlapping curves (Figs. 3b and 3c). These data indicate that exogenous DNA-binding proteins did not change the overall conformation of the *B. subtilis* chromosome. Notably, these exogenous proteins were expressed in the presence of all the native *B. subtilis* proteins. It is possible that *B. subtilis*' own NAPs, like HBsu, robustly organized the chromosome and predominated over the exogenous proteins. Alternatively, these proteins might only alter the local DNA structure at a very short range beyond the resolution of our Hi-C assay, but do not affect the overall folding pattern of the genome.

SMC movement rate is unaffected by the exogenous DNA-binding proteins

Our microscopy and ChIP-seq results showed that the fusion proteins were expressed to a desirable level, localized to the nucleoid, and bound to the DNA with characteristic sequence specificities. To understand whether these proteins affected SMC movement, we measured SMC translocation rates along the genome in the presence or absence of these proteins. The HupA-mCherry/HupB heterodimer, the HMfA-mCherry/HMfB heterodimer, or H-NS-mCherry were expressed under a xylose inducible promoter (Pxyl) for 90 min. Fluorescence images showed that these proteins localized to the nucleoid (**Fig. S2a**) and were expressed at appropriate levels (**Fig. S2b**). Next, SMC loading was induced by expressing ParB protein from an IPTG inducible promoter. In the control strain not expressing exogenous proteins, SMC moved at a speed of 53 ± 2 kb/min, consistent with previous results[10] (Fig. 4a). When the HupA-mCherry/HupB heterodimer, the HMfA-mCherry/HMfB heterodimer, or H-NS-mCherry was expressed, SMC translocation rates were very similar to that of the control, within the range of experimental error (Figs. 4a and 4b). Thus, expression of exogenous DNA-binding proteins did not affect SMC movement, indicating that SMC can easily bypass these proteins in vivo.

To understand whether the lack of effect of DNA-binding proteins on SMC translocation was due to the mCherry tag compromising the function of the proteins, we performed the same experiments in cells expressing untagged H-NS. We first analyzed the genome-wide binding profile of H-NS expressed in *B. subtilis* by ChIP-seq using anti-H-NS antibodies[57]. We found that untagged H-NS had the same enrichment peaks as H-NS-mCherry and as *B. subtilis* WT Rok protein, albeit at slightly lower heights (**Figs. S1c and S1d**), indicating that H-NS and H-NS-mCherry bind to the same locations. In Hi-C experiments, expressing untagged H-NS resulted in the same chromosomal conformation as expressing H-NS-mCherry (**Figs. S1e and S1f.**). Thus, the lack of impact of our fusion proteins on chromosome architecture was not because of the mCherry tag.

Discussion

In this study, we investigated the effects of exogenous DNA-binding proteins on SMC translocation in *B. subtilis*. We chose a collection of bacterial and archaeal DNA-binding proteins that preferentially bind different DNA sequences and act differently on DNA. Using Western Blotting and fluorescence microscopy, we demonstrated that these proteins were expressed to a level higher than or similar to *B. subtilis*' native NAP, HBsu, which has about ~ 20,000 monomers per cell[53]. To avoid cytotoxicity, we did not try higher expression levels. We showed that these proteins were localized to the nucleoid and bound to the genome with enrichment patterns characteristic of the proteins in their native organisms. Using time-resolved Hi-C, we demonstrated that SMC translocation rates remained unchanged in strains expressing these proteins. Together, this work has shown that the processivity of SMC is unaffected by the presence of exogenous DNA-binding proteins on the chromosome.

When exogenous proteins were expressed in *B. subtilis*, we observed no change in chromosome conformation (Fig. 3), but previous studies have shown that HupAB and H-NS play a role in structuring the *E. coli* chromosome[58]. Specifically, HupAB promotes long-range interactions (> 280 kb) outside the *ter* region, whereas H-NS decreases the interactions between its binding sites and the neighboring regions[58]. Similarly, in *Brucella abortus*, an H-NS-like protein MucR also caused local and global changes to chromosome structure[59]. What could be the reason that these NAPs, which play chromosome-structuring roles in their native organisms, have no effects on chromosome conformation when expressed in *B. subtilis*? One possibility is that these DNA-binding proteins work together with other host factors in their native organisms. For instance, in *E. coli*, it was suggested that HupAB's role in promoting DNA contact > 280 kb could be through another protein complex MukBEF[58], which is absent in *B. subtilis*. Another possibility is that our experimental setup concealed the structuring roles of these exogenous proteins because all native *B. subtilis* proteins are present in our strains. We suspect that SMC, HBsu, and all other chromosome-organizing factors have generated a stable and robust chromosome structure and predominated over the exogenous proteins. Despite the lack of effect on global chromosome conformation, these exogenous proteins have bound to the chromosome in a characteristic manner as shown in fluorescence microscopy and ChIP-seq. Thus, they serve our purpose to test the effect of DNA-binding proteins on SMC translocation.

In *B. subtilis*, the SMC complexes that are loaded at the origin can translocate the entire length of the genome and reach the terminus region[8,10]. In this process, SMC must be able to traverse all factors on the nucleoid. Our study shows that when additional DNA-binding proteins are expressed to further crowd the chromatin, SMC translocation rate is unaffected. This finding is not surprising, rather it highlights the robustness and processivity of SMC complexes on the busy chromatin. Recent studies showed that yeast condensins can bypass various DNA-binding proteins and large nanoparticles bound to DNA, but not a dense array of a telomeric protein[28,60]. Thus, some DNA-binding proteins may present challenges or roadblocks for SMC translocation. It will be interesting to determine the specific properties of these proteins that affect SMC movement, such as their binding affinities to DNA, their densities on DNA, the local DNA structures they cause, or the specific functions they perform.
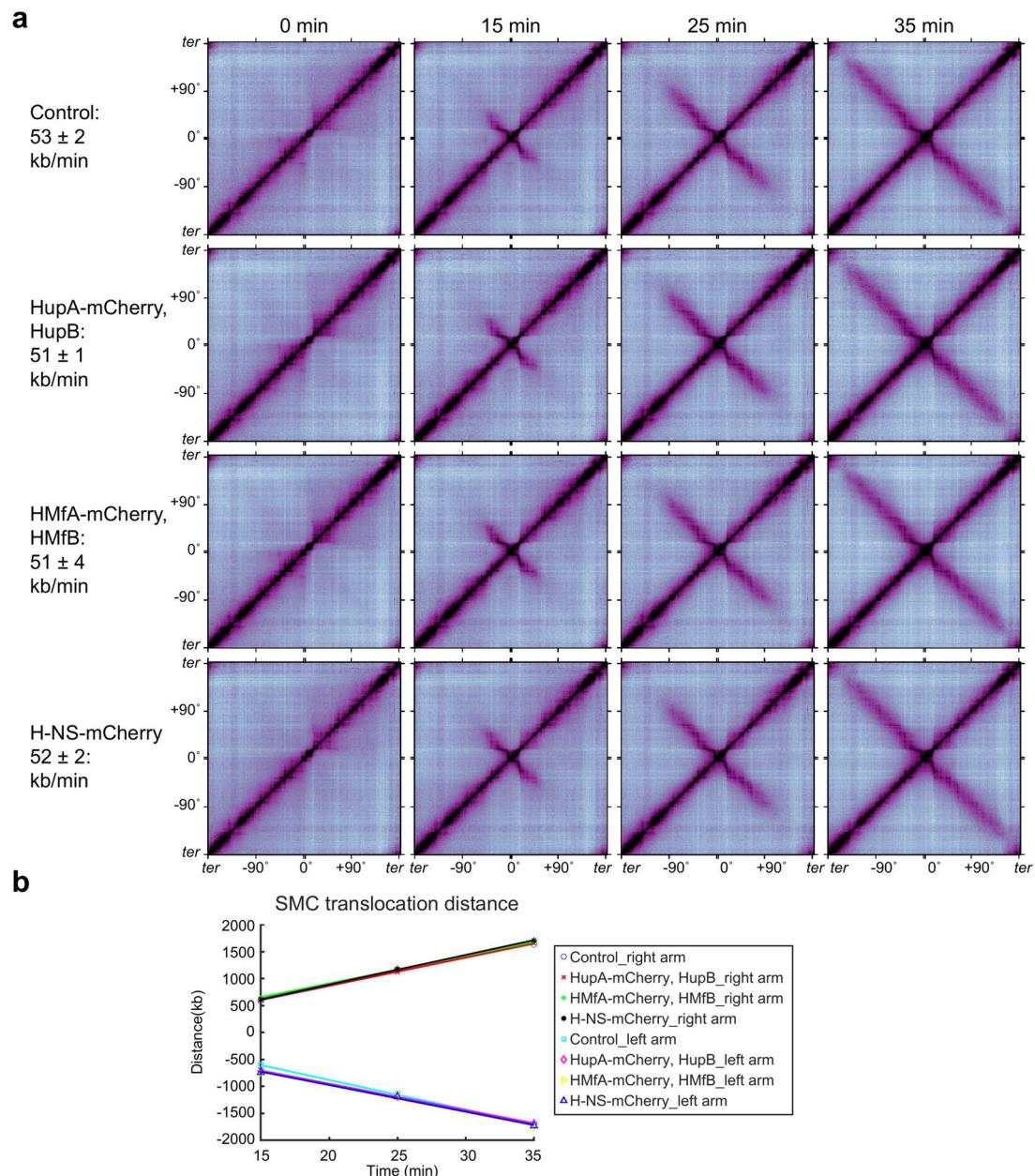
Fig. 4. Effects of exogenous DNA-binding proteins on SMC translocation. (**a**) Hi-C time course after ParB induction. Normalized contact maps for the control strain (BWX4070) and strains expressing indicated proteins: the HupA-mCherry/HupB heterodimer (BWX5602), the HMfA-mCherry/HMfB heterodimer (BWX5603), or H-NS-mCherry (BWX5663). The exogenous DNA-binding proteins were induced with 0.5% xylose for 90 min. Then 0.5 mM IPTG was added to induce the expression of ParB protein. The samples were collected at 0 min, 15 min, 25 min, and 35 min after adding IPTG. The rate of SMC translocation was indicated, as calculated in (**b**). (**b**) Calculation of SMC translocation rate. The x-axis represents the time after inducing ParB. The y-axis represents the distance of juxtaposed DNA. The distance on the right arm was labeled as a positive value, and on the left arm as a negative value. The rates for DNA juxtaposition were calculated from the slope of the line of best fit.

Although SMC translocation is often not affected by DNA-binding proteins, several studies showed that SMC movement can be influenced by various motor proteins. For instance, simulations on Hi-C results suggested that RNA polymerases slow down *B. subtilis* SMC complex and human cohesin in vivo[27,61]; the human minichromosome maintenance (MCM) complex was found to impede cohesin movement both in vivo and in vitro[62]; single-molecule experiments showed that SMC cohesins can be blocked and pushed by the replisome in vitro[63–65]; an in vitro study on yeast condensin[66] and an in vivo study on *B. subtilis* SMC complex[67] showed that when two SMC complexes meet each other on the DNA, they block each other before bypassing one another

or, at a much lower chance, dissociating from the chromosome. Future endeavors are needed to understand the molecular mechanisms underlying these interactions.

Limitations of this study

Here we aimed to understand the effects of various DNA-binding proteins on SMC translocation in *B. subtilis*. All native *B. subtilis* proteins were still present, and the exogenous DNA-binding proteins were expressed in addition. Native NAPs may be predominating over the structure of chromosome, preventing exogenous DNA-binding proteins from significantly changing chromosome organization.

Materials and methods

Experimental model and subject details

Bacterial strains and growth

B. subtilis strains were derived from the prototrophic strain PY79[68]. Cells were grown in defined rich medium (CH)[69] at 37 °C with aeration. Lists of strains, plasmids, oligonucleotides and Next-Generation-Sequencing samples can be found in Tables S1-S4.

Methods details

Immunoblot analysis

Exponentially growing cells were collected and resuspended in lysis buffer (20 mM Tris pH 7.0, 1 mM EDTA, 10 mM $MgCl_2$, 1 mg/ml lysozyme, 10 μg/ml DNase I, 100 μg/ml RNase A, 1 mM PMSF and 1% proteinase inhibitor cocktail (Sigma-Aldrich P-8340, St. Louis, MO)) to a final OD_{600} of 10 for equivalent loading. The cell resuspensions were incubated at 37˚C for 10 min for lysozyme treatment. Then, an equal volume of 2 × Laemmli Sample Buffer (Bio-Rad 1610737, Hercules, CA) containing 10% β-Mercaptoethanol was added. The samples were heated for 5 min at 95˚C before loading. Proteins were separated by precast 4–20% polyacrylamide gradient gels (Bio-Rad 4561096, Hercules, CA). The Bio-Rad Transblot Turbo system and reagents (Bio-Rad 1704156, Hercules, CA) were used to electroblot the proteins onto mini PVDF membranes. The membranes were blocked using 5% nonfat milk in phosphate-buffered saline (PBS) with 0.5% Tween-20 and then probed with rabbit polyclonal anti-mCherry (1:5000)[70], anti-HBsu (1:20,000) (gift from David Rudner) or anti-SigA (1:10,000)[71] diluted into 3% BSA in 1 × PBS-0.05% Tween-20. Primary antibodies were detected by Immun-Star horseradish peroxidase-conjugated goat anti-rabbit antibodies (Bio-Rad 1705046, Hercules, CA) and Western Lightning Plus ECL chemiluminescence reagents using the protocol described by the manufacturer (Perkin Elmer NEL1034001, Waltham, MA). The signal was captured using ProteinSimple Fluorchem R system.

Fluorescence microscopy

Fluorescence microscopy was performed using a Nikon Ti2 microscope (Nikon Instruments, Melville, NY) equipped with Plan Apo 100x/1.45NA phase contrast oil objective and an sCMOS camera. Cells were grown in defined rich Casein Hydrolysate (CH) medium[69] at 37˚C overnight and then were sub-cultured in 25 ml of CH medium at an initial OD_{600} of 0.02. After one hour of sub-culturing, 1 ml of 15% xylose was added to induce the expression of the fluorescently labeled nonspecific DNA-binding proteins. After a 90-min induction, cells were collected for imaging. The cells were immobilized using 2% agarose pads containing CH growth media. Images were cropped and adjusted using Nikon NIS-elements software. Fluorescence intensity was quantified using MetaMorph software (Molecular Devices). Final figure preparation was performed in Adobe Illustrator.

ChIP-seq

Chromatin immunoprecipitation (ChIP) was performed as described previously[7]. Cells were crosslinked using 3% formaldehyde for 30 min at room temperature. The cells were quenched using 125 mM glycine, washed with PBS, and lysed using lysozyme. A Qsonica Q800R2 water bath sonicator was used to shear crosslinked chromatin to an average size of 170 bp. The lysate was precleared using Protein A magnetic beads (GE Healthcare/Cytiva 28,951,378, Marlborough, MA) and then incubated with anti-mCherry[70], anti-HBsu (gift from David Rudner), anti-Rok[72] or anti-H-NS[57] antibodies overnight at 4˚C. The following day, the lysate was incubated with Protein A magnetic beads for 1 h at 4˚C. After washes and elution, the immunoprecipitates was incubated at 65˚C overnight to reverse the crosslinking. The DNA was further treated with RNaseA and Proteinase K, extracted with PCI, resuspended in 100 μl EB, and used for library preparation with the NEBNext Ultra II kit (E7645). Library sequencing was performed using Illumina NextSeq500 or Nextseq2000 (Illumina, San Diego, CA) at the IU Center for Genomics and Bioinformatics. The sequencing reads were mapped to the genome of *B. subtilis* PY79 (NCBI reference sequence NC_022898.1) using CLC Genomics Workbench (Qiagen, Hilden, Germany). Sequencing reads were normalized by the total number of reads, plotted, and analyzed using R.

Whole genome sequencing

The experiments were performed as previously described[67]. Cells were grown in CH medium containing necessary supplements (such as 0.5% xylose) at 37 °C. Samples were collected at the desired time points. Genomic DNA was extracted using the Qiagen DNeasy blood and tissue kit (69,504; Qiagen). DNA was sonicated using a Qsonica Q800L sonicator for 12 min at 20% amplitude to achieve an average fragment size of 170 bp. DNA library was prepared using NEBNext Ultra II kit (E7645; NEB) and sequenced using Illumina NextSeq500 or Nextseq2000. Sequencing reads were mapped to the *B. subtilis* PY79 genome (NCBI reference sequence NC_022898.1) using CLC Genomics Workbench (Qiagen). The mapped reads were normalized to the total number of reads and used as input for the ChIP-samples.

Hi-C

The Hi-C procedure was carried out as previously described[8]. Specifically, cells grown at the desired condition were crosslinked with 3% formaldehyde at room temperature for 30 min then quenched with 125 mM glycine. Cells were lysed using Ready-Lyse Lysozyme (Epicentre, R1802M) and treated by 0.5% SDS. Solubilized chromatin was digested with DpnII for 2 h at 37 ˚C. The digested ends were filled in with Klenow and Biotin-14-dATP, dGTP, dCTP, dTTP. The products were ligated with T4 DNA ligase at 16 ˚C for about 20 h. Crosslinks were reversed at 65 ˚C for about 20 h in the presence of EDTA, proteinase K and 0.5% SDS. The DNA was then extracted twice with phenol/chloroform/isoamylalcohol (PCI 25:24:1), precipitated with ethanol, and resuspended in 20 μl of 0.1XTE buffer. Biotin from non-ligated ends was removed using T4 polymerase (4 h at 20 ˚C) followed by extraction with PCI. The DNA was then sheared by sonication for 12 min with 20% amplitude using a Qsonica Q800R2 water bath sonicator. The sheared DNA was used for library preparation with the NEBNext UltraII kit (E7645). Biotinylated DNA fragments were purified using 10 μl streptavidin beads. DNA-bound beads were used for PCR in a 50 μl reaction for 14 cycles. PCR products were purified using Ampure beads (Beckman, A63881) and sequenced at the Indiana University Center for Genomics and Bioinformatics using NextSeq500 or NextSeq2000. Paired-end sequencing reads were mapped to the genome of *B. subtilis* PY79 (NCBI reference sequence NC_022898.1) using the same pipeline described previously[8]. The *B. subtilis* PY79 genome was first divided into 404 10-kb bins. Subsequent analysis and visualization were done using R scripts. For the $\log_2$ ratio plots, the Hi-C matrix of strain 1 was divided by the matrix of strain 2. Then, $\log_2$(strain 1/strain 2) was calculated and plotted in a heatmap using R. The rates of SMC translocation were calculated using $0.51 \times$ standard deviation as previously described[10].

Plasmid construction

pWX981

[*ycgO::PftsW hns-mcherry phleo*] was generated by a ligation of two gel-purified fragments: 1) pWX510[73] digested by HindIII and XhoI; 2) *hns* amplified using oWX2555 and oWX2556 on the gDNA of *E. coli* MG1655, and then digested by HindIII and XhoI.

pWX991

[*yhdG::Pxyl hns-mcherry phleo*] was constructed by ligation of two gel-purified fragments: 1) pMS025 digested by HindIII and BamHI to give *yhdG::Pxyl phleo* ; 2) pWX981 digested by HindIII and BamHI to give *hns-mcherry*. The construct was sequenced using oML87 and oWX1894.

pWX993

[*yhdG::Pxyl hupA-mcherry phleo*] was constructed by ligation of two gel-purified fragments: 1) pMS025 digested by HindIII and BamHI to give *yhdG::Pxyl phleo* ; 2) pWX1001 (see below) digested by HindIII and BamHI to give *hupA-mcherry*. The construct was sequenced using oML87 and oWX1894.

pWX994

[*yhdG::Pxyl hupB-mcherry phleo*] was constructed by ligation of two gel-purified fragments: 1) pMS025 digested by HindIII and BamHI to give *yhdG::Pxyl phleo* ; 2) pWX1002 (see below) digested by HindIII and BamHI to give *hupB-mcherry*. The construct was sequenced using oML87 and oWX1894.

pWX1001

[*ycgO::PftsW hupA-mcherry phleo*] was generated by a ligation of two gel-purified fragments: 1) pWX510[73] digested by HindIII and XhoI; 2) *hupA* amplified using oWX2559 and oWX2587 on the gDNA of *E. coli* MG1655, and then digested by HindIII and XhoI.

pWX1002

[*ycgO::PftsW hupB-mcherry phleo*] was generated by a ligation of two gel-purified fragments: 1) pWX510[73] digested by HindIII and XhoI; 2) *hupB* amplified using oWX2561 and oWX2588 on the gDNA of *E. coli* MG1655, and then digested by HindIII and XhoI.

pWX1072

[*yhdG::Pxyl hmfA-mcherry phleo*] was constructed by ligation of two gel-purified fragments: 1) pMS025 digested by HindIII and XhoI to give *yhdG::Pxyl mch*erry phleo ; 2) Ec-HMfA plasmid[47] (gift from Tobias Warnecke) amplified by oWX2227 and oWX2903 then digested by HindIII and XhoI to give *hmfA*. The construct was sequenced using oML87 and oWX1894.

pWX1073

[*yhdG::Pxyl hmfB-mcherry phleo*] was constructed by ligation of two gel-purified fragments: 1) pMS025 digested by HindIII and XhoI to give *yhdG::Pxyl mCherry phleo* ; 2) Ec-HMfB plasmid[47] (gift from Tobias Warnecke) amplified by oWX2229 and oWX2904 then digested by HindIII and XhoI to give *hmfB*. The construct was sequenced using oML87 and oWX1894.

pWX1180

[*yuxG::Pxyl hupB erm*] was constructed by isothermal assembly of two gel-purified fragments: 1) pWX146 digested by HindIII and SpeI to give *yuxG::erm* ; 2) pWX994 amplified by oWX3230 and oWX3231 to give *xylR-Pxyl-hupB*. The construct was sequenced using oWX1894. pWX146 is an integration vector that has *yuxG::erm*.

pWX1181

[*yuxG::Pxyl hmfB erm*] was constructed by isothermal assembly of two gel-purified fragments: 1) pWX146 digested by HindIII and SpeI to give *yuxG::erm*; 2) pWX1073 amplified by oWX3232 and oWX3233 to give *xylR-Pxyl-hmfB*. The construct was sequenced using oWX1894. pWX146 is an integration vector that has *yuxG::erm*.

pWX1182

[*yhdG::Pxyl mcherry phleo*] was constructed by isothermal assembly of two gel-purified fragments 1) pMS025 digested by HindIII and BamHI to give *yhdG::Pxyl* phleo ; 2) pWX985 amplified using oWX3234 and oWX3235 to give *mcherry*. The construct was sequenced using oWX1894.

pWX1252

[*yhdG::Pxyl hns phleo*] was constructed by ligation of two gel-purified fragments: 1) pMS025 digested by HindIII and BamHI to give *yhdG::Pxyl phleo* ; 2) *hns* amplified using oWX2555 and oWX3573 on the gDNA of *E. coli* MG1655, and then digested by HindIII and BamHI. The construct was sequenced using oWX486 and oWX2493.

pWX1270

[*yhdG::Pxyl nbhmfA-mcherry phleo*] was constructed by ligation of two gel-purified fragments: 1) pWX991 digested by HindIII and XhoI to give *yhdg::Pxyl mcherry phleo*; 2) *nbhmfA* amplified using oWX2231 and oWX3649 on Ec-nbHMfA plasmid[47] (gift from Tobias Warnecke), and then digested by HindIII and XhoI. The construct was sequenced by oML87 and oWX1894.

pWX1271

[*yhdG::Pxyl nbhmfB-mcherry phleo*] was constructed by ligation of two gel-purified fragments: 1) pWX991 digested by HindIII and XhoI to give *yhdg::Pxyl mcherry phleo*; 2) *nbhmfA* amplified using oWX2233 and oWX3650 on Ec-nbHMfA plasmid[47] (gift from Tobias Warnecke), and then digested by HindIII and XhoI. The construct was sequenced by oML87 and oWX1894.

Strain construction

BWX523

[*sacA::hbsu-mcherry kan*] was constructed by direct transformation of a two-way ligation into *B. subtilis*, which inserts the *hbs* gene with its native promoter (amplified using primers odr198 and odr214 and digested with EcoRI and BamHI) into pWX345 between EcoRI and BamHI. pWX345 contains *sacA::mcherry (kan)*.

Other *B. subtilis* strains used in this study were generated by transforming the plasmids described above, or by successive transformation of *B. subtilis* genomic DNA.

Data availability

Unprocessed microscopy images are available at Mendeley data: https://data.mendeley.com/datasets/y46hk46c24/3. Hi-C, ChIP-seq and WGS data were deposited to the NCBI Gene Expression Omnibus (https://www.ncbi.nlm.nih.gov/geo/query/acc.cgi?acc=GSE269767). The scripts used for plotting and analyses were deposited to https://github.com/xindanwanglab/Ren-2024-SMC-NAP. Any additional information required to analyze the data reported in this paper is available from the Corresponding Author upon request without restriction. Further information and requests for resources and reagents should be directed to and will be fulfilled by the Corresponding Author.

Materials availability

Plasmids and strains generated in this study are available from the Corresponding Author with a completed Materials Transfer Agreement.

References

1. Uhlmann, F. SMC complexes: from DNA to chromosomes. *Nat. Rev. Mol. Cell Biol.* **17**, 399–412. https://doi.org/10.1038/nrm.2016.30 (2016).
2. Yatskevich, S., Rhodes, J. & Nasmyth, K. Organization of chromosomal DNA by SMC complexes. *Annu. Rev. Genet.* **53**, 445–482. https://doi.org/10.1146/annurev-genet-112618-043633 (2019).
3. Unal, E. et al. A molecular determinant for the establishment of sister chromatid cohesion. *Science* **321**, 566–569. https://doi.org/10.1126/science.1157880 (2008).
4. Schwarzer, W. et al. Two independent modes of chromatin organization revealed by cohesin removal. *Nature* **551**, 51–56. https://doi.org/10.1038/nature24281 (2017).
5. Hirano, T. Condensin-based chromosome organization from bacteria to vertebrates. *Cell* **164**, 847–857. https://doi.org/10.1016/j.cell.2016.01.033 (2016).
6. Kong, M. et al. Human condensin i and ii drive extensive atp-dependent compaction of nucleosome-bound DNA. *Mol. Cell* **79**(99–114), e119. https://doi.org/10.1016/j.molcel.2020.04.026 (2020).
7. Wang, X., Tang, O. W., Riley, E. P. & Rudner, D. Z. The SMC condensin complex is required for origin segregation in Bacillus subtilis. *Curr. Biol.* **24**, 287–292. https://doi.org/10.1016/j.cub.2013.11.050 (2014).
8. Wang, X. et al. Condensin promotes the juxtaposition of DNA flanking its loading site in bacillus subtilis. *Genes Dev.* **29**, 1661–1675. https://doi.org/10.1101/gad.265876.115 (2015).
9. Tran, N. T., Laub, M. T. & Le, T. B. K. SMC progressively aligns chromosomal arms in caulobacter crescentus but is antagonized by convergent transcription. *Cell Rep.* **20**, 2057–2071. https://doi.org/10.1016/j.celrep.2017.08.026 (2017).

10. Wang, X., Brandao, H. B., Le, T. B., Laub, M. T. & Rudner, D. Z. Bacillus subtilis SMC complexes juxtapose chromosome arms as they travel from origin to terminus. *Science* **355**, 524–527. https://doi.org/10.1126/science.aai8982 (2017).
11. Bock, F. P., Liu, H. W., Anchimiuk, A., Diebold-Durand, M. L. & Gruber, S. A joint-ParB interface promotes Smc DNA recruitment. *Cell Rep.* **40**, 111273. https://doi.org/10.1016/j.celrep.2022.111273 (2022).
12. Takemata, N., Samson, R. Y. & Bell, S. D. Physical and functional compartmentalization of archaeal chromosomes. *Cell* **179**(165–179), e118. https://doi.org/10.1016/j.cell.2019.08.036 (2019).
13. Sanborn, A. L. et al. Chromatin extrusion explains key features of loop and domain formation in wild-type and engineered genomes. *Proc. Natl. Acad. Sci. U S A* **112**, E6456-6465. https://doi.org/10.1073/pnas.1518552112 (2015).
14. Hassler, M., Shaltiel, I. A. & Haering, C. H. Towards a unified model of SMC complex function. *Curr. Biol.* **28**, R1266–R1281. https://doi.org/10.1016/j.cub.2018.08.034 (2018).
15. Marko, J. F., De Los Rios, P., Barducci, A. & Gruber, S. DNA-segment-capture model for loop extrusion by structural maintenance of chromosome (SMC) protein complexes. *Nucleic Acids Res.* **47**, 6956–6972. https://doi.org/10.1093/nar/gkz497 (2019).
16. Gruber, S. & Errington, J. Recruitment of condensin to replication origin regions by ParB/SpoOJ promotes chromosome segregation in B. subtilis. *Cell* **137**, 685–696. https://doi.org/10.1016/j.cell.2009.02.035 (2009).
17. Sullivan, N. L., Marquis, K. A. & Rudner, D. Z. Recruitment of SMC by ParB-parS organizes the origin region and promotes efficient chromosome segregation. *Cell* **137**, 697–707. https://doi.org/10.1016/j.cell.2009.04.044 (2009).
18. Wilhelm, L. et al. SMC condensin entraps chromosomal DNA by an ATP hydrolysis dependent loading mechanism in bacillus subtilis. *Elife* https://doi.org/10.7554/eLife.06659 (2015).
19. Marbouty, M. et al. Condensin- and replication-mediated bacterial chromosome folding and origin condensation revealed by Hi-C and super-resolution imaging. *Mol. Cell* **59**, 588–602. https://doi.org/10.1016/j.molcel.2015.07.020 (2015).
20. Wang, X. et al. In vivo evidence for ATPase-dependent DNA translocation by the bacillus subtilis SMC condensin complex. *Mol. Cell* **71**(841–847), e845. https://doi.org/10.1016/j.molcel.2018.07.006 (2018).
21. Ganji, M. et al. Real-time imaging of DNA loop extrusion by condensin. *Science* **360**, 102–105. https://doi.org/10.1126/science.aar7831 (2018).
22. Davidson, I. F. et al. DNA loop extrusion by human cohesin. *Science* **366**, 1338–1345. https://doi.org/10.1126/science.aaz3418 (2019).
23. Kim, Y., Shi, Z., Zhang, H., Finkelstein, I. J. & Yu, H. Human cohesin compacts DNA by loop extrusion. *Science* **366**, 1345–1349. https://doi.org/10.1126/science.aaz4475 (2019).
24. Pradhan, B. et al. The Smc5/6 complex is a DNA loop-extruding motor. *Nature* **616**, 843–848. https://doi.org/10.1038/s41586-023-05963-3 (2023).
25. Terakawa, T. et al. The condensin complex is a mechanochemical motor that translocates along DNA. *Science* **358**, 672–676. https://doi.org/10.1126/science.aan6516 (2017).
26. Pradhan, B. et al. Loop-extrusion-mediated plasmid DNA cleavage by the bacterial SMC Wadjet complex. *Mol. Cell* https://doi.org/10.1016/j.molcel.2024.11.002 (2024).
27. Brandao, H. B. et al. RNA polymerases as moving barriers to condensin loop extrusion. *Proc. Natl. Acad. Sci. U S A* **116**, 20489–20499. https://doi.org/10.1073/pnas.1907009116 (2019).
28. Analikwu, B. T. et al. Telomere protein arrays stall DNA loop extrusion by condensin. *BioRxiv* https://doi.org/10.1101/2023.10.29.564563 (2023).
29. Rouviere-Yaniv, J. & Gros, F. Characterization of a novel, low-molecular-weight DNA-binding protein from Escherichia coli. *Proc. Natl. Acad. Sci. U S A* **72**, 3428–3432. https://doi.org/10.1073/pnas.72.9.3428 (1975).
30. Claret, L. & Rouviere-Yaniv, J. Variation in HU composition during growth of Escherichia coli: the heterodimer is required for long term survival. *J. Mol. Biol.* **273**, 93–104. https://doi.org/10.1006/jmbi.1997.1310 (1997).
31. Broyles, S. S. & Pettijohn, D. E. Interaction of the escherichia coli HU protein with DNA. Evidence for formation of nucleosome-like structures with altered DNA helical pitch. *J. Mol. Biol.* **187**, 47–60. https://doi.org/10.1016/0022-2836(86)90405-5 (1986).
32. Luijsterburg, M. S., White, M. F., van Driel, R. & Dame, R. T. The major architects of chromatin: architectural proteins in bacteria, archaea and eukaryotes. *Crit. Rev. Biochem. Mol. Biol.* **43**, 393–418. https://doi.org/10.1080/10409230802528488 (2008).
33. Luijsterburg, M. S., Noom, M. C., Wuite, G. J. & Dame, R. T. The architectural role of nucleoid-associated proteins in the organization of bacterial chromatin: a molecular perspective. *J. Struct. Biol.* **156**, 262–272. https://doi.org/10.1016/j.jsb.2006.05.006 (2006).
34. van Noort, J., Verbrugge, S., Goosen, N., Dekker, C. & Dame, R. T. Dual architectural roles of HU: Formation of flexible hinges and rigid filaments. *Proc. Natl Acad. Sci.* **101**, 6969–6974. https://doi.org/10.1073/pnas.0308230101 (2004).
35. Hammel, M. et al. HU multimerization shift controls nucleoid compaction. *Sci. Adv.* **2**, e1600650. https://doi.org/10.1126/sciadv.1600650 (2016).
36. Gordon, B. R. et al. Structural basis for recognition of AT-rich DNA by unrelated xenogeneic silencing proteins. *Proc. Natl. Acad. Sci. U S A* **108**, 10690–10695. https://doi.org/10.1073/pnas.1102544108 (2011).
37. Arold, S. T., Leonard, P. G., Parkinson, G. N. & Ladbury, J. E. H-NS forms a superhelical protein scaffold for DNA condensation. *Proc. Natl. Acad. Sci. U S A* **107**, 15728–15732. https://doi.org/10.1073/pnas.1006966107 (2010).
38. Liu, Y., Chen, H., Kenney, L. J. & Yan, J. A divalent switch drives H-NS/DNA-binding conformations between stiffening and bridging modes. *Genes Dev.* **24**, 339–344. https://doi.org/10.1101/gad.1883510 (2010).
39. Dame, R. T., Wyman, C. & Goosen, N. H-NS mediated compaction of DNA visualised by atomic force microscopy. *Nucleic Acids Res.* **28**, 3504–3510. https://doi.org/10.1093/nar/28.18.3504 (2000).
40. Kotlajich, M. V. et al. Bridged filaments of histone-like nucleoid structuring protein pause RNA polymerase and aid termination in bacteria. *Elife* https://doi.org/10.7554/eLife.04970 (2015).
41. Dorman, C. J. H-NS: A universal regulator for a dynamic genome. *Nat. Rev. Microbiol.* **2**, 391–400. https://doi.org/10.1038/nrmicro883 (2004).
42. Marc, F., Sandman, K., Lurz, R. & Reeve, J. N. Archaeal histone tetramerization determines DNA affinity and the direction of DNA supercoiling. *J. Biol. Chem.* **277**, 30879–30886. https://doi.org/10.1074/jbc.M203674200 (2002).
43. Mattiroli, F. et al. Structure of histone-based chromatin in archaea. *Science* **357**, 609–612. https://doi.org/10.1126/science.aaj1849 (2017).
44. Henneman, B. et al. Mechanical and structural properties of archaeal hypernucleosomes. *Nucleic Acids Res.* **49**, 4338–4349. https://doi.org/10.1093/nar/gkaa1196 (2021).
45. Musgrave, D. R., Sandman, K. M. & Reeve, J. N. DNA binding by the archaeal histone HMf results in positive supercoiling. *Proc. Natl. Acad. Sci. U S A* **88**, 10397–10401. https://doi.org/10.1073/pnas.88.23.10397 (1991).
46. Pereira, S. L., Grayling, R. A., Lurz, R. & Reeve, J. N. Archaeal nucleosomes. *Proc. Natl. Acad. Sci. U S A* **94**, 12633–12637. https://doi.org/10.1073/pnas.94.23.12633 (1997).
47. Rojec, M., Hocher, A., Stevens, K. M., Merkenschlager, M. & Warnecke, T. Chromatinization of escherichia coli with archaeal histones. *Elife* https://doi.org/10.7554/eLife.49038 (2019).
48. Hustmyer, C. M. & Landick, R. Bacterial chromatin proteins, transcription, and DNA topology: Inseparable partners in the control of gene expression. *Mol. Microbiol.* **122**, 81–112. https://doi.org/10.1111/mmi.15283 (2024).
49. Dame, R. T., Rashid, F. M. & Grainger, D. C. Chromosome organization in bacteria: Mechanistic insights into genome structure and function. *Nat. Rev. Genet.* **21**, 227–242. https://doi.org/10.1038/s41576-019-0185-4 (2020).

50. Micka, B. & Marahiel, M. A. The DNA-binding protein HBsu is essential for normal growth and development in bacillus subtilis. *Biochimie* **74**, 641–650. https://doi.org/10.1016/0300-9084(92)90136-3 (1992).
51. Kohler, P. & Marahiel, M. A. Association of the histone-like protein HBsu with the nucleoid of bacillus subtilis. *J. Bacteriol.* **179**, 2060–2064. https://doi.org/10.1128/jb.179.6.2060-2064.1997 (1997).
52. Johnson, G. E., Lalanne, J. B., Peters, M. L. & Li, G. W. Functionally uncoupled transcription-translation in bacillus subtilis. *Nature* **585**, 124–128. https://doi.org/10.1038/s41586-020-2638-5 (2020).
53. Le Hegarat, F., Salti-Montesanto, V., Hauck, Y. & Hirschbein, L. Purification and characterization of the HU-like protein HPB9 from the bacillus subtilis nucleoid. *Biochim. Biophys. Acta.* **1172**, 101–107. https://doi.org/10.1016/0167-4781(93)90275-i (1993).
54. Soares, D. J., Sandman, K. & Reeve, J. N. Mutational analysis of archaeal histone-DNA interactions. *J. Mol. Biol.* **297**, 39–47. https://doi.org/10.1006/jmbi.2000.3546 (2000).
55. Teytelman, L., Thurtle, D. M., Rine, J. & van Oudenaarden, A. Highly expressed loci are vulnerable to misleading ChIP localization of multiple unrelated proteins. *Proc. Natl. Acad. Sci. U S A* **110**, 18602–18607. https://doi.org/10.1073/pnas.1316064110 (2013).
56. Hoa, T. T., Tortosa, P., Albano, M. & Dubnau, D. Rok (YkuW) regulates genetic competence in bacillus subtilis by directly repressing comK. *Mol. Microbiol.* **43**, 15–26. https://doi.org/10.1046/j.1365-2958.2002.02727.x (2002).
57. Hustmyer, C. M., Wolfe, M. B., Welch, R. A. & Landick, R. RfaH counter-silences inhibition of transcript elongation by h-ns-stpa nucleoprotein filaments in pathogenic escherichia coli. *MBio* https://doi.org/10.1128/mbio.02662-22 (2022).
58. Lioy, V. S. et al. Multiscale structuring of the E. coli chromosome by nucleoid-associated and condensin proteins. *Cell* **172**, 771–783. https://doi.org/10.1016/j.cell.2017.12.027 (2018).
59. Barton, I. S. et al. Brucella MucR acts as an H-NS-like protein to silence virulence genes and structure the nucleoid. *MBio* https://doi.org/10.1128/mbio.02201-23 (2023).
60. Pradhan, B. et al. SMC complexes can traverse physical roadblocks bigger than their ring size. *Cell Rep.* **41**, 111491. https://doi.org/10.1016/j.celrep.2022.111491 (2022).
61. Banigan, E. J. et al. Transcription shapes 3D chromatin organization by interacting with loop extrusion. *Proc. Natl. Acad. Sci. U S A* **120**, e2210480120. https://doi.org/10.1073/pnas.2210480120 (2023).
62. Dequeker, B. J. H. et al. MCM complexes are barriers that restrict cohesin-mediated loop extrusion. *Nature* **606**, 197–203. https://doi.org/10.1038/s41586-022-04730-0 (2022).
63. Cameron, G. et al. Sister chromatid cohesion establishment during DNA replication termination. *Science* **384**, 119–124. https://doi.org/10.1126/science.adf0224 (2024).
64. Kanke, M. et al. Cohesin acetylation and Wapl-Pds5 oppositely regulate translocation of cohesin along DNA. *EMBO J.* **35**, 2686–2698. https://doi.org/10.15252/embj.201695756 (2016).
65. Glaser, S., Molodtsov, M. I., Diffley, J. F. X. & Uhlmann, F. Replisome passage through the cohesin ring. *BioRxiv* **6**, 7304. https://doi.org/10.1101/2024.10.30.621121 (2024).
66. Kim, E., Kerssemakers, J., Shaltiel, I. A., Haering, C. H. & Dekker, C. DNA-loop extruding condensin complexes can traverse one another. *Nature* **579**, 438–442. https://doi.org/10.1038/s41586-020-2067-5 (2020).
67. Brandao, H. B., Ren, Z., Karaboja, X., Mirny, L. A. & Wang, X. DNA-loop-extruding SMC complexes can traverse one another in vivo. *Nat. Struct. Mol. Biol.* **28**, 642–651. https://doi.org/10.1038/s41594-021-00626-1 (2021).
68. Youngman, P. J., Perkins, J. B. & Losick, R. Genetic transposition and insertional mutagenesis in bacillus subtilis with streptococcus faecalis transposon Tn917. *Proc. Natl. Acad. Sci. U S A* **80**, 2305–2309. https://doi.org/10.1073/pnas.80.8.2305 (1983).
69. Harwood, C. R. & Cutting, S. M. *Molecular biological methods for Bacillus* (Wiley, New York, 1990).
70. Rodrigues, C. D., Ramirez-Guadiana, F. H., Meeske, A. J., Wang, X. & Rudner, D. Z. GerM is required to assemble the basal platform of the SpoIIIA-SpoIIQ transenvelope complex during sporulation in bacillus subtilis. *Mol. Microbiol.* **102**, 260–273. https://doi.org/10.1111/mmi.13457 (2016).
71. Fujita, M. Temporal and selective association of multiple sigma factors with RNA polymerase during sporulation in bacillus subtilis. *Genes Cells* **5**, 79–88. https://doi.org/10.1046/j.1365-2443.2000.00307.x (2000).
72. Seid, C. A., Smith, J. L. & Grossman, A. D. Genetic and biochemical interactions between the bacterial replication initiator DnaA and the nucleoid-associated protein rok in bacillus subtilis. *Mol. Microbiol.* **103**, 798–817. https://doi.org/10.1111/mmi.13590 (2017).
73. Wang, X., Montero Llopis, P. & Rudner, D. Z. Bacillus subtilis chromosome organization oscillates between two distinct patterns. *Proc. Natl. Acad. Sci. U S A* **111**, 12877–12882. https://doi.org/10.1073/pnas.1407461111 (2014).

Acknowledgements

Author contributions

Z.R. and X.W. designed the study; Z.R. and L.E.W. constructed plasmids and strains. L.E.W. performed microscopy and immunoblot experiments and analyses and collected samples for ChIP-seq and Hi-C. Z.R. performed Hi-C and ChIP-seq experiments and analyses. Z.R., L.E.W., and X.W. wrote the manuscript. X.W. supervised the study.

Funding

Declaration

Competing interests

The authors declare no competing interests.

Additional information

Supplementary Information The online version contains supplementary material available at https://doi.org/10.1038/s41598-025-86946-4.

Correspondence and requests for materials should be addressed to X.W.

Reprints and permissions information is available at www.nature.com/reprints.

Publisher's note Springer Nature remains neutral with regard to jurisdictional claims in published maps and institutional affiliations.